INSTITUTE OF PHYSICS PUBLISHING NANOTECHNOLOGY
Nanotechnology **15** (2004) S672–S677 PII: S0957-4484(04)77554-6

Rapid assembly of carbon nanotubes for nanosensing by dielectrophoretic force

Rosa H M Chan, Carmen K M Fung and Wen J Li[1]

Centre for Micro and Nano Systems, The Chinese University of Hong Kong, Hong Kong SAR

E-mail: wen@acae.cuhk.edu.hk

Received 9 March 2004
Published 20 August 2004
Online at stacks.iop.org/Nano/15/S672
doi:10.1088/0957-4484/15/10/028

Abstract
The carbon nanotube (CNT) has been widely studied for its electrical, mechanical, and chemical properties since its discovery. However, to manipulate these nanosize tubes, atomic force microscopy (AFM) is typically used to manipulate them one-by-one. This is time-consuming and unrealistic for batch fabrication. In this paper, we will present the manipulation of carbon nanotubes using dielectrophoretic manipulation to rapidly build practical nanosensors. Thus far, we have demonstrated thermal sensors for temperature and fluid-flow measurements. We have also shown that this electrokinetic based manipulation technique is compatible with MEMS fabrication processes, and hence, MEMS structures embedded with carbon nanotube sensing elements can be built in the future with new functionalities.

(Some figures in this article are in colour only in the electronic version)

1. Introduction

Researchers have recently demonstrated various novel methods in carbon nanotube (CNT) manipulation using guided CNT growth [1, 2], external forces [3, 4], and polar molecular patterning [5]. Whereas the former refined technique grows organized CNT structures (directed assembly) by chemical-vapour deposition, the latter two methods are for pre-grown nanotubes. In the case of external forces, forces generated by electric field, magnetic field and liquid flow have been applied to align and orient CNT arrays. For example, DC or low frequency AC electric field can attract the nanotubes to electrodes quickly and will have enhanced alignment with higher frequency electric field. On the other hand, thick films of nanotubes exhibiting in-plane preferred orientation have been produced by filter deposition from suspension in strong magnetic fields [3]. Microchannels have also been fabricated for fluidic assembly of nanotubes layer-by-layer [4]. Furthermore, polar molecular marks, which are patterned by nanolithography or microcontact stamping, were demonstrated to attract the nanotubes within 10 s [5]. This high yield and high precision method could even connect over 70% of junctions by individual nanotubes. However, an electric field is still better in isolating, aligning and connecting the metallic CNTs for nanoscale circuits congruently, while the semiconducting CNTs for transistors or the impurities will be left in a suspension [6].

Using the technique of electric-field assisted assembly, i.e., dielectrophoresis (DEP) [7], we have successfully manipulated *bundled* multi-walled CNTs (MWNTs) to connect between arrays of microelectrodes. We have demonstrated that pre-grown CNT alignments can be simply controlled by different electrode configurations. Our experimental results agree well with computer simulations that modelled the connections of nanotubes between various electrode configurations in different DEP force fields. Accordingly, DEP makes the batch fabrication of nanodevices using nanotubes as components feasible. In addition, we have proven that CNT devices built by this method are capable of performing very low power thermal sensing (i.e., ∼1000 times lower than conventional MEMS polysilicon based thermal sensors) and can be fabricated in a fast and efficient manner [8]. The detailed process to manipulate nanotubes using a DEP force and the experimental results from using the CNT bundles as thermal sensing elements will be presented in this paper.

[1] Author to whom any correspondence should be addressed.

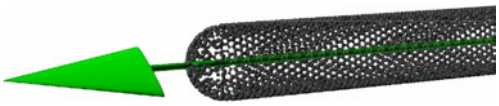

Figure 1. Assume that the carbon nanotube is a long prolate spheroid such as a cigar in shape; its longest axis aligns with the electric field direction (arrow) in DEP.

2. Dielectrophoretic manipulation of CNTs

In our CNT manipulation experiments, the CNTs were dispersed inside a liquid medium (e.g., ethanol); therefore forces (e.g., viscous forces) other than the dielectrophoretic forces are also imparted on the CNTs during the manipulation process. In order to understand the physical phenomenon during the dielectrophoretic manipulation, we conducted the following simulations on the effect of different microelectrode geometries on CNT alignments. The results were also validated experimentally.

2.1. Theory

During the CNT manipulation, the total force acting on an MWNT is the sum of a number of independent forces [9, 10]. With negligible gravitational force, the three main force components are the DEP force, the viscous force and the electrothermal force. For other small particles with their volumes compatible to MWNTs, the thermal effects can dominate, but the high polarizability of MWNTs makes the DEP force large enough to produce the deterministic movements close to the electrode gap. Thus, the depositions between adjacent electrode edges are dominated by DEP.

Dielectrophoresis refers to the force exerted on a polarized particle in a non-uniform electric field [7]. It can be written as

$$\boldsymbol{F}_{\mathrm{DEP}}(t) = (\boldsymbol{m}(t) \cdot \nabla)\boldsymbol{E}(t) \tag{1}$$

where $\boldsymbol{E}$ is the electric field, and $\boldsymbol{m}$ is the induced dipole moment of MWNT. Assuming that the MWNT is a long prolate spheroid with the longest axis aligned with the electric field, the induced dipole moment is

$$\boldsymbol{m}(t) = 4\pi\varepsilon_{\mathrm{m}} a b^2 K \boldsymbol{E}(t) \tag{2}$$

where ε_{m}, a and b are the absolute permittivity of the medium, the half length of the MWNT and the radius of the MWNT, respectively. The complex polarization factor K is given by

$$K = \frac{\varepsilon_{\mathrm{p}}^* - \varepsilon_{\mathrm{m}}^*}{3[\varepsilon_{\mathrm{m}}^* + (\varepsilon_{\mathrm{p}}^* - \varepsilon_{\mathrm{m}}^*)L_{\parallel}]} \tag{3}$$

where $\varepsilon_{\mathrm{p}}^*$ and $\varepsilon_{\mathrm{m}}^*$ are the absolute complex permittivities of the MWNT [11] and the medium ethanol [12], respectively, while the approximated depolarization factor [7] $L_{\parallel}$ is $\approx (b^2/a^2)[\ln(2a/b) - 1]$. Since the electric field components are in phase, the time averaged DEP force deduced from the above equations is

$$\langle \boldsymbol{F}_{\mathrm{DEP}}(t) \rangle = 2\pi a b^2 \varepsilon_{\mathrm{m}} \,\mathrm{Re}(K) \nabla |\boldsymbol{E}_{\mathrm{rms}}|^2 \tag{4}$$

where $\nabla|\boldsymbol{E}_{\mathrm{rms}}|^2$ is the gradient of the square of the root-mean-square of the electric field. The gradient is affected by both the geometry of the electrodes and the applied voltage. The former factor gives the overall position of the MWNT branches between the electrodes because it determines the direction of the average DEP force. As the potential difference applied is proportional to the magnitude of electric field, a larger potential can increase the magnitude of the DEP force and offer a larger torque to align the MWNTs with the electric field direction as in figure 1 [7]. The smaller the gaps, the larger the change in electric field for the same magnitude of voltage applied, thus the force is stronger.

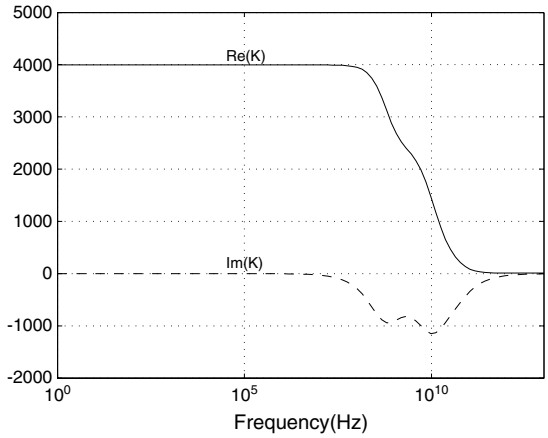

Figure 2. Complex polarization factor K when the longest axis of the MWNT is parallel to the electric field applied.

The frequency of the applied voltage also affects the magnitude of the DEP force since the complex permittivity spectra of MWNTs and ethanol are functions of the frequency. Because of the high conductivity of the assumed purified MWNT ($\approx 2.22 \times 10^4$ S m^{-1}) [11] and the small depolarization factor resulting from its long dipole ($L_{\parallel} \approx 8.3434 \times 10^{-5}$), the real part of the complex polarization factor is positive, as shown in figure 2. Alternatively, to calculate the DEP force when the longest axis of the CNT is perpendicular to the field by (4), the new complex polarization factor $\mathrm{Re}(K) \approx 0.6667$ is obtained by substituting $L_{\parallel}$ by $L_{\perp} \approx 0.5$ in (3). The corresponding positive dielectrophoretic forces draw the MWNT to the electric field maxima.

Another factor affecting the magnitude of the force is the volume of the MWNT as shown in (4). In the MWNT manipulation experiments, MWNTs with axial length and diameter about 1–10 μm and 10–30 nm, respectively, were used. Therefore, $a = 2.5$ μm and $b = 10$ nm were taken for the average size of the CNTs simulated.

To validate the simulation results, detailed experimental procedures in forming CNT bundles across microelectrodes will be presented in section 2.3. In order to visualize the electric field distribution generated by different microelectrode geometries, simulations have been conducted and they are described in the following section.

2.2. Simulations

Consider the DEP setup with thin gold electrodes on a substrate that lies in an aqueous CNT suspension. The simulation first involves solving the Laplace equation, $\nabla^2\Phi = 0$, for the

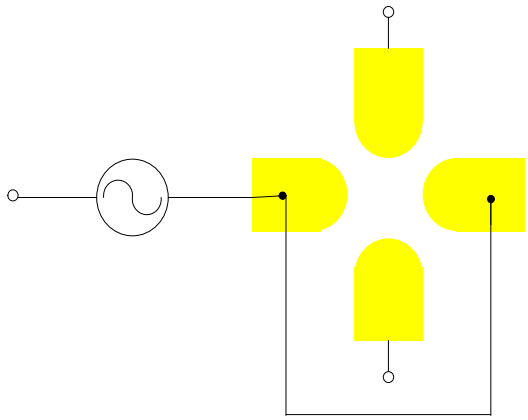

Figure 3. Electrode configuration for test and the respective application of electrical potential. The same 1 MHz 16 V peak-to-peak AC was applied on an opposite set of electrodes. Their adjacent electrodes were free-ended.

potential Φ to derive the electrical field $\boldsymbol{E}$. This is a non-trivial problem for complicated microelectrode geometries. However, Wang *et al* [13] have introduced the application of the Green theorem to solve the Laplace equation and transform the problem into one of integration. At the point $r_0 = (x_0, y_0, z_0)$,

$$\Phi(r_0) = \frac{1}{4\pi} \int \frac{2z_0 \Phi(z = 0)}{[(x - x_0) + (y - y_0) + z_0]^{3/2}} \, \mathrm{d}x \, \mathrm{d}y \qquad (5)$$

where $\Phi(z = 0)$ is the boundary condition, i.e., electrode surface plane potential.

Despite the common usage in deriving analytical expressions for the electrical fields of respective specific geometries (e.g., an array of parallel electrodes), numerical calculations of the integral equation (5) are conducted for complicated electrode geometries where analytical expressions are not available. The estimated error parameter resulting from the numerical method was defined by Wang *et al* as the ratio of the studied position height h to the smallest one-dimensional size of the studied features l. When the parameter $h/l < 10\%$, the field can be assumed accurate. Otherwise, the definite area of the electrode plane potential to be studied should be increased.

As an illustration, the electrode configuration as in figure 3 was designed. The approximate order of the potential was then investigated by using the Green theorem [13], and the square root-mean-square magnitude of the field was calculated by using MatLab. Since the magnitude of the electric field decreases with height from the electrodes, the positive DEP draws the MWNT downwards to the edges of the electrodes. The force fields in figure 4 are estimated by (4), assuming that the longest axis of the MWNT is parallel to the instantaneous electric field. Downward DEP forces are shown by the contours in between the electrodes and close to the electrode surfaces. Therefore, the force vector diagrams for different electrode geometries can be simulated [14] and thus the alignments of CNTs to be deposited by dielectrophoresis can be approximated beforehand.

The time averaged alignment torque acting on the MWNTs causes them to have the longest axis directed as the electric field vectors as demonstrated in figure 1. As the electric field intensity is higher at the closest corners

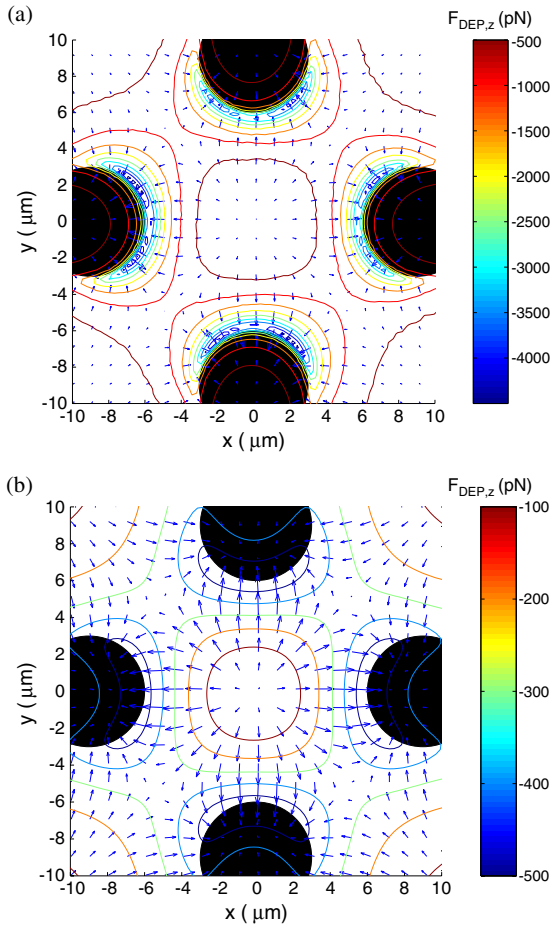

Figure 4. Average DEP force between the electrodes as in figure 3. The arrows are the force vectors on the x–y plane (a) at 1 μm and (b) 3 μm, respectively, above the electrodes in figure 5. The contours represent the order of downward forces.

between electrodes, the MWNTs are drawn to their edge. When an MWNT touches one of the electrodes, it shares the same potential as the electrode and thus the electric field intensity is modified to be higher at its free end. Therefore, the nanotubes near the charged one tend to stick to it. When the nanotube bridges the adjacent voltages, branching structures between electrodes are formed [15]. And strong interaction between the nanotube and the surface via van der Waals forces [16] makes the carbon nanotubes stay where they have been placed. Details of the experimental procedures for the dielectrophoretic manipulation of MWNTs are presented in the next section.

2.3. Experimental verification of theory

Based on the physical phenomenon of dielectrophoresis, we have successfully manipulated bundled CNTs onto microfabricated microelectrodes. The experimental process flow for CNT manipulation can be divided into fabrication of microelectrodes, sample preparation and experimental testing.

Gold microelectrodes were fabricated on Si/SiO_2 substrates by a standard microfabrication technique, which was described and demonstrated previously in [17]. Prior to the MWNT manipulation, bundled MWNTs were prepared

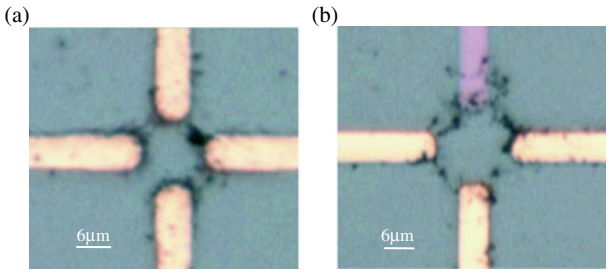

Figure 5. Experimental alignments of MWNT branches when (a) the voltage was applied as in figure 3. The top electrode of (b) was torn while the MWNTs were still in place, demonstrating the strong adhesion of MWNTs on the substrate after deposition.

by ultrasonic dispersion. The bundled MWNTs used in the experiments were ordered commercially from [18], and were prepared by chemical vapour deposition. The samples consisted of both metallic and semiconducting nanotubes. The axial dimension and the diameter of the MWNTs were 1–10 μm and 10–30 nm, respectively. In order to minimize the degree of aggregation, 50 mg of the sample was ultrasonically dispersed in 500 ml ethanol solution and the resulting solution was diluted to 0.01 mg ml^{-1} for later usage.

During the CNT manipulation, a substrate with fabricated gold microelectrodes was placed on the vacuum pump based stage of a micromanipulator station, which allowed the probing of microelectrodes by microprobes. The microelectrodes were then excited by an AC voltage source typically of 16 V peak-to-peak with frequency of 1 MHz. Approximately 10 μl of the MWNT/ethanol solution was transferred to the substrate by a 6 ml gas syringe. The ethanol was evaporated away in a few seconds, leaving the MWNTs to reside between the gaps of the microelectrodes. We observed from the experimental results that bundled MWNTs were attracted towards the microelectrodes under non-uniform electric field and connected across the microelectrodes as in simulations.

The connectivity of CNT bridges between electrodes was proven by electrical conductivity tests. The two probe room temperature resistances of the samples typically ranged from several kΩ to several hundred kΩ, which suggested that the connection had been formed between the two microelectrodes.

Since the resistivity of CNTs depends on their lattice geometries during their growth process, the conductivities of individual CNTs cannot be well controlled, which results in the variation of conductivities in individual CNTs. During the AC electrophoresis process to form MWNT bundles across microelectrodes, the MWNTs were randomly connected between microelectrodes. Therefore, it is logical that different MWNT samples exhibited different conductivities.

We have found that the results were repeatable for different chips with the same electrode configurations and the mode of voltage applied as demonstrated by the consistent Wheatstone bridge alignments in figure 5.

The asymmetrical amounts of MWNTs deposited above were due to the random dispersion of MWNTs in the ethanol resulting in an asynchronous deposition. However, the overall alignments matched with the simulation in general. In order to have fewer bundled MWNTs deposited in between the electrodes, we could have a more diluted MWNT/ethanol suspension used. Nonetheless, the potential of failed MWNT connection in between adjacent electrodes would be increased as well.

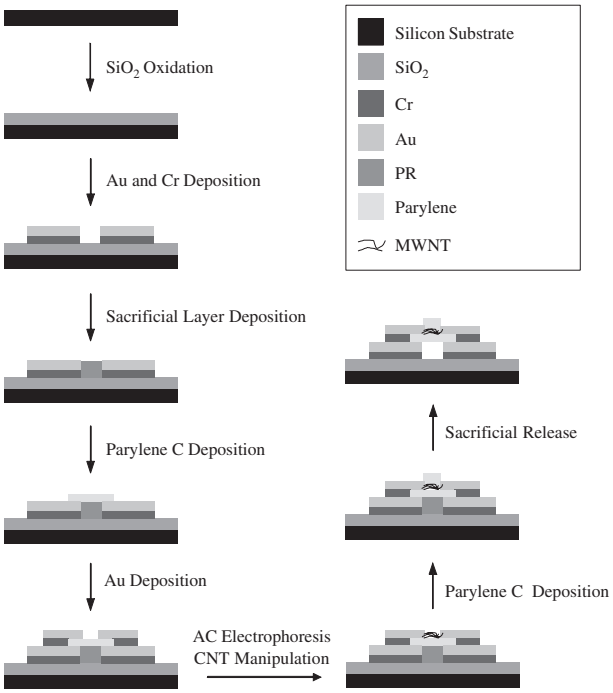

Figure 6. Fabrication process flow for the CNT based MEMS sensor.

3. CNTs as sensing elements

3.1. Fabrication process

We have demonstrated in our work [17] that bundled CNTs can be used as a novel material for microthermal sensing applications. We have also found that the devices can be operated at the μW range, which is ultra-low power consumption for applications like shear stress and thermal sensing (e.g., in the order of mW range for typically MEMS polysilicon devices [20]). However, in our previous work, the MWNT devices were exposed to air, and there was no direct means to fix the MWNT bundles on electrodes, except by van der Waals forces. Therefore, in order to protect the CNTs from contamination and to better secure them to the electrodes, a MEMS-compatible process was developed to encapsulate the MWNT bundles for reliable test and measurements.

The fabrication process for the CNT embedded sensor is shown in figure 6. A parylene C polymer was used to embed the bulk MWNTs. The advantage of using parylene C is that it can be deposited conformably at room temperature. As seen in the fabrication process, SiO_2 was first deposited on the silicon substrate to avoid conduction of the gold electrode with the substrate. Then the Au and Cr electrodes were patterned on the substrate (Cr was used to improve the adhesion of Au to the substrate). Photoresist (AZ5214) was spun-on and patterned between the Au electrodes to provide a trench under the MWNT sensor. This photoresist layer could be used as a sacrificial layer for particular applications of the sensors. The bottom parylene C layer was then deposited on the substrate to

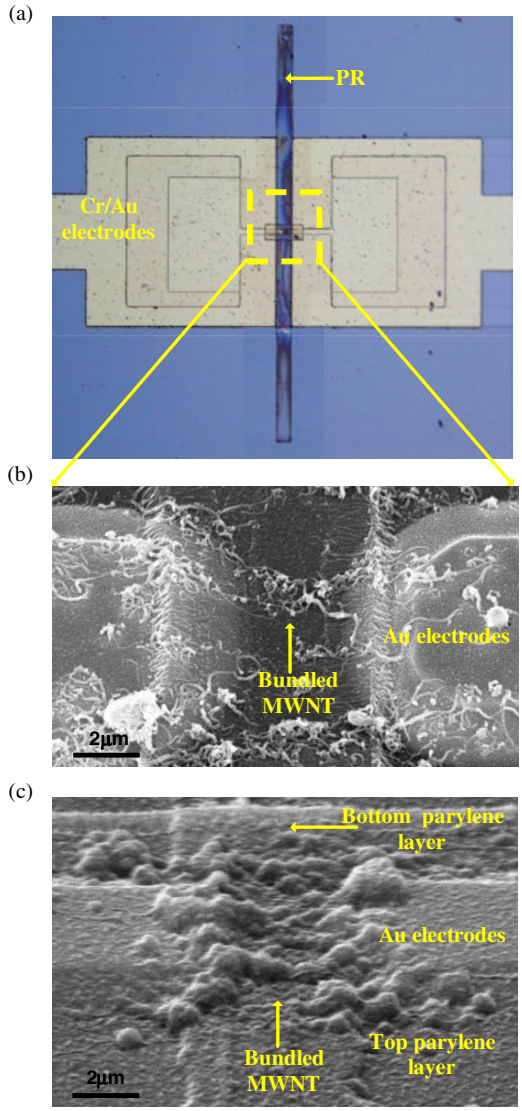

Figure 7. (a) Optical microscopic image showing the prototype parylene/MWNT/parylene sensor. (b) and (c) Scanning electron microscopic (SEM) images showing that the bundled MWNTs were formed on top of the parylene C layer and were embedded inside the parylene C layers, respectively.

isolate the MWNT bundles from the substrate. In order to form the bulk MWNT on the top of the parylene C layer effectively, additional Au microelectrodes were patterned on the top of the bottom parylene C layer. This provided a small gap distance to allow the CNT manipulation more efficiently. This gap distance for the CNT sensor was between 3 and 10 μm. Based on the technique for CNT manipulation presented in the previous section, the bundled MWNTs were manipulated and connected across the microelectrodes of each sensor (by observing the resistance change between the electrodes). Afterwards, the top parylene C layer was deposited to embed the MWNTs and protect them from contamination. Finally, the sacrificial layer was released to serve as mechanical microbridges that suspend the MWNT sensors across the Au electrodes. An optical microscopic image of the fabricated MWNT sensor is shown in figure 7.

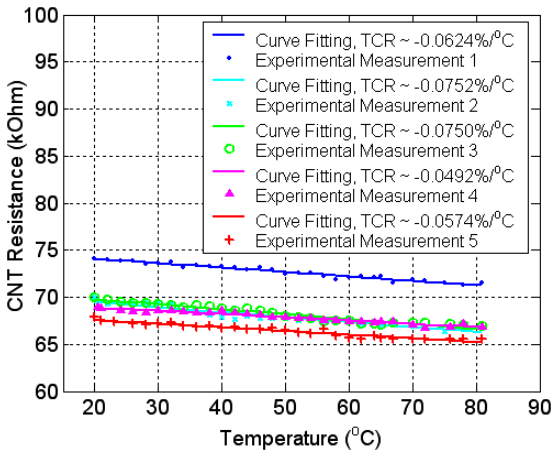

Figure 8. TCR for a parylene/MWNT/parylene sensor in five different measurements.

3.2. Thermal sensitivity

We have investigated the possibility to utilize the bundled CNTs as sensing elements for thermal sensing. Compared to the results collected for the unencapsulated MWNT devices reported in [17], the resistance for these embedded CNT sensors is more stable and consistent.

Bundled MWNTs as sensing elements for microthermal sensors can be driven by a simple constant current circuit. An experiment for investigating the temperature dependence of the bulk MWNT sensor was performed. The fabricated sensor chip was packaged on a PCB for data acquisition and was put inside an oven. Then, the resistance change of the MWNT sensors was measured as the temperature inside the oven was varied. The temperature–resistance relationship for the MWNT sensors was measured and a representative data set is shown in figure 8 for several cycles of measurements. From the experimental results, the bundled MWNT resistance dropped with temperature. Other than the first measurement cycle, the resistance at room temperature converged and the slopes were consistent for each measurement. The negative temperature coefficient of resistance (TCR) of the MWNTs had been reported previously in [19], although the measurements were based on individual MWNTs. As reported in [19], the variations in resistivities and temperature resistance dependency of CNTs are due to the interplay of changes in carrier concentration and mobilities in the metallic tubes. Therefore, the linear relationship of the resistance and temperature of our bundled CNT sensor can be predicted and the behaviour of resistance decreasing with increasing temperature is possibly dependent on the intrinsic thermal properties of the MWNTs. The temperature–resistance dependency of bundled MWNTs implies their thermal sensing capability. By observing the drift in resistance for the first measurement, we concluded that the MWNT sensors become stable after a temperature annealing process. Based on experimental results, the range of the TCR for the MWNT sensors was found to be from -0.04 to -0.07% $^{\circ}\mathrm{C}^{-1}$.

Comparing with the drift in the room temperature resistance and convergence of data from measurement of different temperature ramping cycles reported in [17], the performance of current parylene encapsulated MWNT sensors

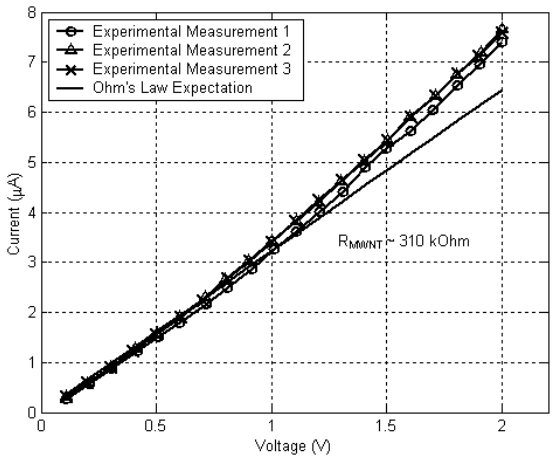

Figure 9. *I–V* characteristics of a parylene/MWNT/parylene sensor. Three repeated measurements were performed to validate its repeatability. The straight line is the theoretical expectation using Ohm's law. The room temperature resistance of bundled MWNTs of this sample was about 310 kΩ.

is more stable and consistent. With parylene protecting the MWNT linkage between the microelectrodes, these new MWNT based MEMS sensors will have much fewer contaminations such as moisture and dust particles during measurements, and will also prevent the MWNTs from detaching from the Au electrodes even if the sensors undergo thermal cycling.

3.3. Power consumption

The *I–V* characteristic of the MWNT sensors was also investigated. From the results of experiments conducted on the MWNT sensors, the current required to induce self-heating of the MWNT devices was in the μA range at several volts, which suggests that the power consumption of these devices is in the μW range (see figure 9).

4. Conclusion

A technique to batch fabricate nanosensors using CNTs based on dielectrophoretic manipulation was presented. We have proven that an AC electric field can direct MWNTs to specific areas of patterned substrates. With specially designed microelectrodes, bundled MWNTs can be aligned into different directions according to the electric field generation. The simulation results for the electric field distribution for different designs of microelectrode geometries were also presented.

With the ability to manipulate the bundled MWNTs onto microelectrodes, bundled MWNTs were investigated as a sensing element for microthermal sensing applications. Due to the ultra-low power consumption of the bundled MWNTs, they should be promising in thermal sensing applications. With parylene encapsulation, these novel sensors will have much fewer contaminations, and in addition will not have carbon nanotubes detaching from the electrodes even if the sensors undergo thermal cycling. The performances of our current parylene encapsulated MWNT sensors are also proven to be more stable and consistent.

Acknowledgment

The authors would like to sincerely thank Dr W Y Cheung of the Department of Electronic Engineering of CUHK for his help and discussion on this project.

References

[1] Wei B Q, Vajtai R, Jung Y, Ward J, Zhang R, Ramanath G and Ajayan P M 2002 *Nature* **416** 495–6
[2] Hu J, Ouyang M, Yang P and Lieber C M 1999 *Nature* **399** 48–51
[3] Fischer J E, Zhou W, Vavro J, Llaguno M C, Guthy C, Haggenmueller R, Casavant M J, Walters D E and Smalley R E 2003 *J. Appl. Phys.* **93** 2157–63
[4] Huang Y, Duan X, Wei Q and Lieber C M 2001 *Science* **291** 630–3
[5] Rao S G, Huang L, Setyawan W and Hong S 2003 *Nature* **425** 36–7
[6] Krupke R, Hennrich F, Löhneysen H v and Kappes M M 2003 *Science* **301** 344–7
[7] Jones T B 1995 *Electromechanics of Particles* (Cambridge: Cambridge University Press)
[8] Fung C K M and Li W J 2003 *Proc. IEEE NANO* **2** 866–9
[9] Heida T, Rutten W L C and Marani E 2002 *J. Phys. D: Appl. Phys.* **35** 1592–602
[10] Ramos A, Morgan H, Green N G and Castellanos A 1998 *J. Phys. D: Appl. Phys.* **31** 2338–53
[11] Grimes C A, Dickey E C, Mungle C, Ong K G and Qian D 1995 *J. Appl. Phys.* **90** 4134–7
[12] Petong P, Pottel R and Kaatze U 2000 *J. Phys. Chem.* A **104** 7420–8
[13] Wang X, Wang X-B, Becker F F and Gascoyne P R C 1996 *J. Phys. D: Appl. Phys.* **29** 1649–60
[14] Chan R H M, Fung C K M and Li W J 2003 *Workshop Lecture Notes, IEEE/RSJ IROS (31 October 2003)*
[15] Yamamoto K, Akita S and Nakayama Y 1996 *Japan. J. Appl. Phys.* **35** L917–8
[16] Hertel T, Martel R and Avouris P 1998 *J. Phys. Chem.* B **102** 910–5
[17] Wong V T S and Li W J 2003 *Proc. IEEE MEMS 2003* 41–4
[18] Sun Nanotech Co. Ltd, Beijing, P.R., China
[19] Ebbesen T W, Lezec H J, Hiura H, Bennett J W, Ghaemi H F and Thio T 1996 Electrical conductivity of individual carbon nanotubes *Nature* **382** 54–6
[20] Liu C, Huang J B, Zhu Z, Jiang F, Tung S, Tai Y C and Ho C M 1999 *J. Microelectromech. Syst.* **8** 90–9